iScience

CellPress
OPEN ACCESS

Article

Alzheimer's-specific brain amyloid interactome: Neural-network analysis of intra-aggregate crosslinking identifies novel drug targets

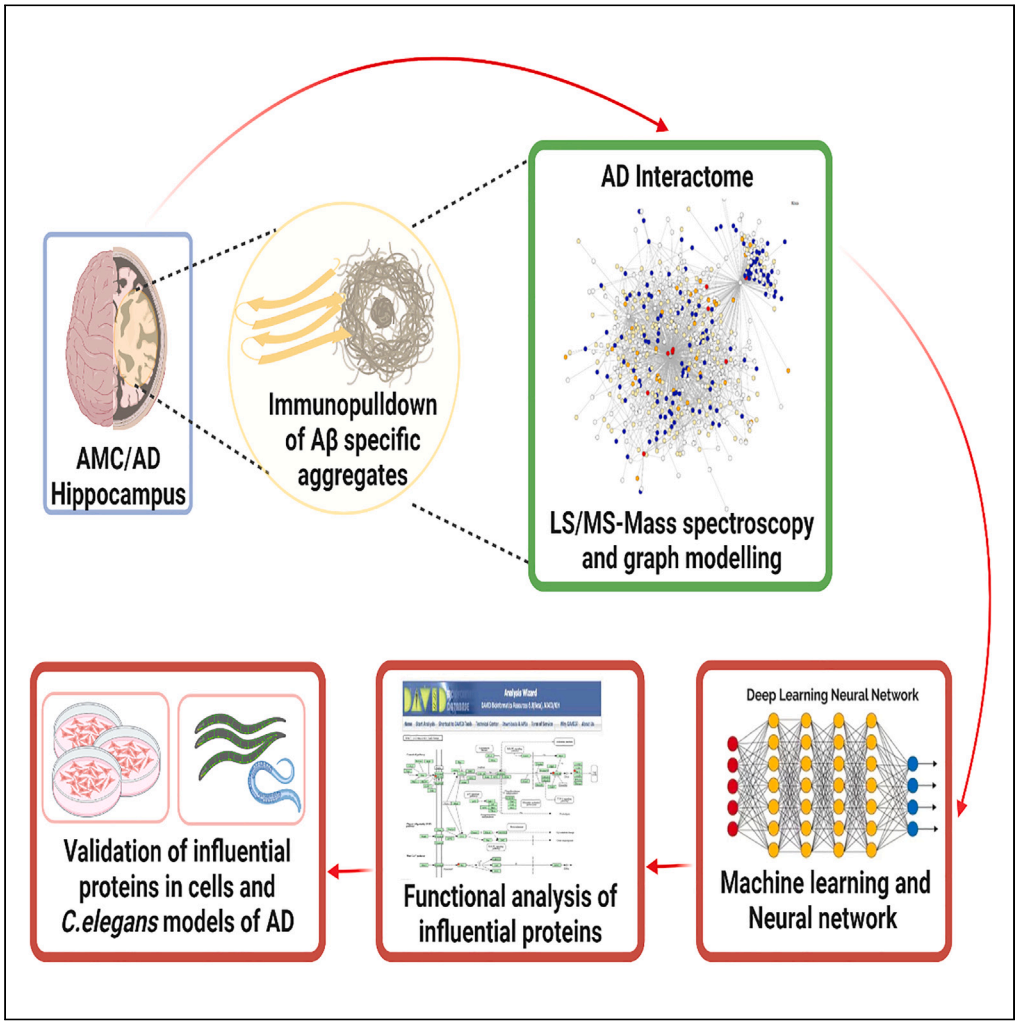

Meenakshisundaram Balasubramaniam, Akshatha Ganne, Nirjal Mainali, Sonu Pahal, Srinivas Ayyadevara, Robert J. Shmookler Reis

mbalasubramaniam@uams.edu (M.B.)
ayyadevarasrinivas@uams.edu (S.A.)
rjsr@uams.edu (R.J.S.R.)

Highlights

AD-specific interactomes predict proteins influential in disease progression

AD aggregate cross-links establish the preferred sequence of protein aggregation

Experimental tests of predicted key proteins confirm their aggregation influence

Mitochondrial and cytoplasmic GO terms are highly enriched in AD aggregate proteins

Balasubramaniam et al., iScience 27, 108745
January 19, 2024
https://doi.org/10.1016/j.isci.2023.108745

iScience

CellPress
OPEN ACCESS

Article

Alzheimer's-specific brain amyloid interactome: Neural-network analysis of intra-aggregate crosslinking identifies novel drug targets

Meenakshisundaram Balasubramaniam,[1,*] Akshatha Ganne,[1] Nirjal Mainali,[2] Sonu Pahal,[2] Srinivas Ayyadevara,[1,3,*] and Robert J. Shmookler Reis[1,3,4,*]

SUMMARY

Alzheimer's disease (AD) is characterized by peri-neuronal amyloid plaque and intra-neuronal neurofibrillary tangles. These aggregates are identified by the immunodetection of "seed" proteins ($A\beta_{1-42}$ and hyperphosphorylated tau, respectively), but include many other proteins incorporated nonrandomly. Using click-chemistry intra-aggregate crosslinking, we previously modeled amyloid "contactomes" in SY5Y-APP_{Sw} neuroblastoma cells, revealing that aspirin impedes aggregate growth and complexity. By an analogous strategy, we now construct amyloid-specific aggregate interactomes of AD and age-matched-control hippocampi. Comparing these interactomes reveals AD-specific interactions, from which neural-network (NN) analyses predict proteins with the highest impact on pathogenic aggregate formation and/or stability. RNAi knockdowns of implicated proteins, in *C. elegans* and human-cell-culture models of AD, validated those predictions. Gene-Ontology meta-analysis of AD-enriched influential proteins highlighted the involvement of mitochondrial and cytoplasmic compartments in AD-specific aggregation. This approach derives dynamic consensus models of aggregate growth and architecture, implicating highly influential proteins as new targets to disrupt amyloid accrual in the AD brain.

INTRODUCTION

Neurotoxic inclusions, comprising intra-neuronal and extracellular aggregates, are critical hallmark features of diverse neurodegenerative diseases including Alzheimer's disease (AD) and Parkinson's disease (PD). Aggregates from AD tissue comprise "seed" or initiator proteins (e.g., $A\beta_{1-42}$ and hyperphosphoryated tau fragments[1]), augmented by a wide variety of other proteins, most of which feature high levels of disorder.[2–5] Among the most abundant aggregate constituents are 14-3-3 paralogs, α-synuclein, neurofilament and motor proteins, hyperphosphorylated tau, Glial Fibrillary Acidic Protein (GFAP), and TAR DNA Binding Protein (TDP-43), which have been identified in diverse aggregates isolated by immuno-pulldown with antibodies to Aβ, tau, or α-synuclein.[5,6] Knockdown of some of these commonly aggregating proteins in *C. elegans* models of neurodegenerative aggregation, including models of AD, PD, and Huntington's disease, indicate highly leveraged roles of these proteins in aggregate formation and stability.[2,5,7,8] Moreover, proteins recovered from neurodegenerative disease aggregates show marked enrichment for post-translational modifications (PTMs) such as phosphorylation, acetylation, and oxidation of residues that are pristine in normal controls.[5,7] PTMs may induce structural changes that alter the functional activities of a protein while at the same time exposing buried surfaces (predominantly hydrophobic) that favor aggregate adhesion. We recently showed that GFAP co-aggregates with both tau and Aβ "seed" proteins in Alzheimer aggregates, and is fully (>95%) phosphorylated at sites that remain unmodified (<5%) in age-matched-control (AMC) aggregates.[5] Knockdown of GFAP in diverse neurodegeneration model systems conferred significant protection against aggregation, as did a small molecule (drug candidate) that directly and selectively targets GFAP.[5] Similarly, we previously showed that 14-3-3 paralogs, especially 14-3-3γ (14-3-3G or gamma), interact preferentially with hyperphosphorylated tau, present only in AD aggregates.[9] This demonstrates the need to delineate aggregate architecture specific for each neurodegenerative disease, to understand the etiology of aggregate formation and to identify new therapeutic targets and drugs to combat these diseases.

We previously established an interactome-modeling approach in which crosslinking was used to derive aggregate-specific "contactomes" for insoluble aggregates from SH-SY5Y-APP_{Sw} cells, a human neuroblastoma model of amyloidopathy associated with familial AD.[10] Graph modeling and neural-network analysis identified critical hub and hub-connector proteins that play key roles in aggregate accretion and insolubility.[10] Accurate prediction of highly influential proteins, based on knockdown-mediated protection against aggregate accrual, provides a

[1]Department of Geriatrics, Reynolds Institute on Aging, University of Arkansas for Medical Sciences, Little Rock, AR 72205, USA
[2]Bioinformatics Program, University of Arkansas for Medical Sciences and University of Arkansas at Little Rock, Little Rock, AR 72205, USA
[3]McClellan Veterans Medical Center, Central Arkansas Veterans Healthcare Service, Little Rock, AR 72205, USA
[4]Lead contact
*Correspondence: mbalasubramaniam@uams.edu (M.B.), ayyadevarasrinivas@uams.edu (S.A.), rjsr@uams.edu (R.J.S.R.)
https://doi.org/10.1016/j.isci.2023.108745

powerful strategy to assess or confirm the importance of specific protein-protein interactions. Applying machine learning (including neural networks) to analyze empirical data, we predicted influential proteins that play crucial roles in protein aggregation.[10]

As a proof-of-principle example, we assessed a known inhibitor of protein aggregation, aspirin,[11,12] showing that it significantly reduced the complexity of insoluble aggregates in SH-SY5Y-APP$_{Sw}$ human neuroblastoma cells.[10] Aspirin is a prolific acetyl donor for many aggregation-prone proteins, including HSP90.[10,13] Aspirin markedly reduced protein recruitment into aggregates, supporting the strategy of mapping the aggregate interactome to identify targets that may disrupt aggregation.[5,11] Our preferred term for the aggregate interactome is "contactome," because its internal crosslinks reflect the protein-protein adhesion architecture within aggregates, but are unlikely to reflect functional interactions. This approach provides a mechanistic basis for predicting and disrupting protein aggregation, by identifying key "lynchpin" proteins that can serve as potential therapeutic targets for drug discovery.

In the present work, we used the same interactome-modeling approach to analyze β-amyloid aggregates isolated from AD and AMC hippocampi. We combine empirical data from chemical crosslinking within aggregates, and graph modeling based on those inputs, to assess the validity of neural-network (NN) predictions based on wet-lab determinations of aggregate abatement after knockdown of key targets in human-cell or *C. elegans* models of neurodegenerative aggregation, by siRNA or RNAi respectively. We first constructed aggregate-specific protein contact networks of sarcosyl-insoluble aggregates from AD brain tissues vs. their AMC counterparts. The non-functional protein-protein contacts that we describe here are highly nonrandom, and define disease-specific interactomes that govern the growth and stability of Aβ plaque, as well as tau tangles and other aggregates in AD brains.

RESULTS

Interactome modeling of Aβ-specific insoluble aggregates from Alzheimer's disease brains

To construct the intra-aggregate contactome (protein-protein interface network) from AD hippocampi, aggregates were isolated from 3 individual AD samples and 3 age-matched-control (AMC) samples, as previously described[7]; see Table S1. Aggregates are known to be quite heterogeneous,[4,7,14] so we first isolated relatively pure populations of AD aggregates by immuno-pulldown (IP) with antibodies to AD-specific "seed" proteins, in this case antibody to human Aβ$_{1–42}$, and these were cross-linked using our published protocol.[7] In brief, after 100,000 x g centrifugation to recover sarcosyl-insoluble aggregates from an Aβ$_{1–42}$-IP, pellets were permeated with a cross-linking reagent and a biotin-tagged linker, which were coupled by azido-alkyne cyclo-addition. After mild tryptic digestion, cross-linked peptide pairs are recovered on streptavidin-coated magnetic beads, released, and analyzed by mass spectrometry (see STAR methods for details), yielding high-resolution m/z data that were interrogated with a modified version of Xlink Identifier.[10,15] Linked peptide pairs are *prima facie* evidence of a protein-protein interface that might contribute to the aggregate contactome network. Two stringency criteria were imposed to exclude or minimize random interactions and false positives, and thus to reduce the complexity of the insoluble-aggregate consensus interactome derived from hippocampal samples: crosslinked peptide pairs were required (***i.***) to have >5 spectral hits per individual sample, and (***ii.***) to be present in all three individual AD brain-aggregate samples, but absent or far less abundant in AMC samples. To aid visualization, proteins (nodes) with fewer than two additional interacting partners were pruned from the network, retaining only the total number of links (edges) for the preceding hub.

Based on these filters, identified protein-protein pairs were analyzed for the following network-based descriptors using GePhi graph-modeling software[10,16] and an in-house R script: (***i.***) the "degree" (number of directly interacting partners) of each node protein; (***ii.***) the clustering coefficient (CC) of the full network; (***iii.***) the eigenvector centrality (EC) of the network; and (***iv.***) the number of triangles (linked triads) in the network. To differentiate disease (AD)-specific aggregates from normal, non-pathognomonic aggregates, we compared Aβ-specific consensus contactomes from 3 AD vs. 3 age-matched control (AMC) hippocampi, applying the same constraints as noted above. Cross-linking and interactome analysis of the AD-specific Aβ$_{1-42}$-aggregate interactome identified 1,325 proteins (nodes) involved in 47,808 interactions, for a mean of 72 interactions per node if all hubs are weighted equally (Figure 1A [degree]). The Aβ$_{1-42}$-aggregate interactome for AMC samples identified 29,733 interactions for 1,369 nodes (a mean of 44 interactions/node, all hubs weighted equally). The average number of interacting partners per node is thus 64% higher in the AD interactome than in AMC ($P < 1E{-}24$, 2-tailed *t* test). The number of triangles (triads of three interconnected nodes), a measure of aggregate complexity,[10,17,18] is 2.5-fold greater for the AD interactome than AMC ($P < 1E{-}4$, 2-tailed *t* test; Figure 1B [triangles]).

To prioritize AD-specific protein-protein interactions that could serve as therapeutic targets for protein-protein interaction inhibitors (PPIIs), we calculated common edges (interactions) shared between AD and AMC aggregates. Of 47,808 AD interactions, only 7,304 (15%) were also present in AMC. Thus, although protein aggregation occurs progressively with age in many organisms and in multiple mammalian tissues,[2–4,7,19,20] AD amyloid-specific aggregates are far more abundant and complex than age-dependent aggregates observed in AMC brains (Figure 1C, total edges per individual interactome, n = 3; $p < 0.04$ by 2-tailed heteroscedastic *t* test). As a tool for the discovery of proteins that are preferentially aggregated in AD relative to AMC, we calculated the ***degree ratio*** (ratio of interacting partners, AD/AMC). We developed an R-based graph-visualization tool to indicate individual hubs and their degrees (numbers of "contactome" direct connections). The resulting graph (Figure 1D) thus emphasizes nodes in the Aβ-specific interactome of AD aggregates, for which AD degree greatly exceeded AMC degree. In this panel, red color denotes proteins that had at least 4-fold more direct (first-degree) contacts in AD aggregates than in AMC. Since these aggregates are immuno-purified for Aβ peptides, we extracted just the direct-interaction partners of peptide Aβ (sometimes called "A4") to create the subnetwork shown in Figure 1E.

The AD aggregate contactome revealed a complex architecture comprising ~1300 proteins, engaged in 1.9-fold more interactions than were observed in AMC aggregates. AD nodes can be partitioned based on the number of interacting partners (degree) of each,[10] as 323

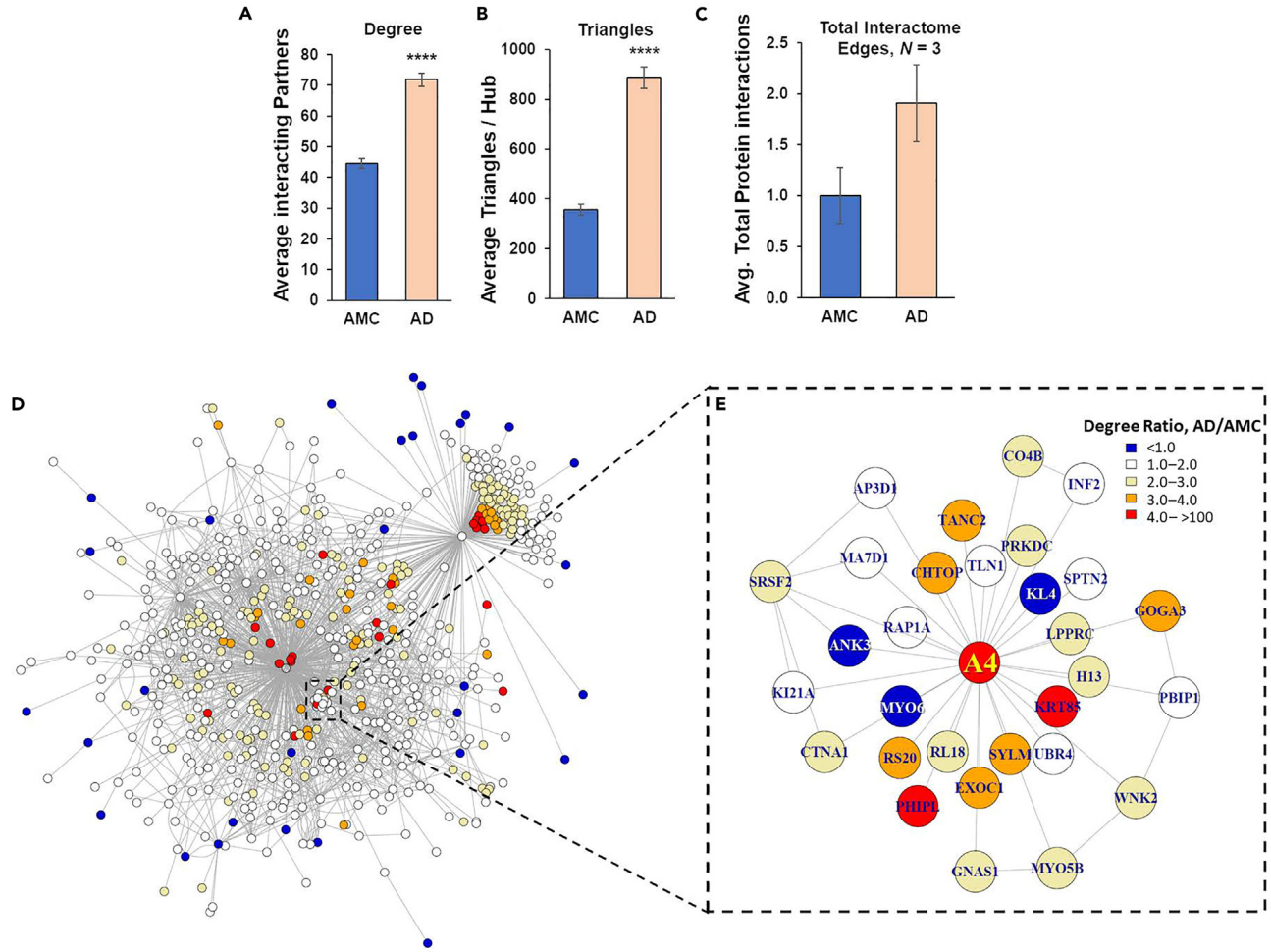

Figure 1. Crosslinking of AD vs AMC hippocampal aggregates defines the Aβ-specific contactome

(A) Mean degree (number of interacting partners) of nodes in insoluble-aggregate contactomes from AD and AMC hippocampi, derived by crosslinking analysis of aggregates isolated by Aβ-immuno-pulldown (Aβ-IP).

(B) Mean number of triangles (ternary associations) per node in insoluble-aggregate contactomes from AD vs. AMC hippocampi, derived by crosslinking analysis of aggregates isolated by Aβ-IP.

(C) Mean number of protein-protein interactions (PPI), summed over the entire aggregate contactome derived by crosslinking analysis of Aβ-IP-isolated aggregates from AD vs. AMC hippocampi, treating each individual as a single data point.

(A–C) Error bars show means ±SEM. ****$p < 6E{-}82$ by 2-tailed homoscedastic *t* tests.

(D) Graph-model representation of the insoluble-aggregate contactome from AD hippocampal samples. Node colors indicate the AD/AMC degree ratios (see key insert in panel E): orange and red nodes indicate the highest differential connectivity (AD/AMC) at 3–4 and 4–100, respectively.

(E) Direct contacts (first-degree interacting partners) of Aβ peptide in AD insoluble aggregates, showing the degree enrichment ratio for AD/AMC aggregates (see key resources table).

mega-hubs (>100 partners), 296 major hubs (50–99 partners), 498 midi-hubs (10–49 partners), 11 mini-hubs (2–9 partners; clustering coefficient [CC] > 0.5), and 195 "hub connectors" (2–9 partners; CC/EC < 100, where EC is eigenvector centrality). The size distributions of hub proteins for AD aggregate interactome are shown in Figure 2A. It is noteworthy that most mega-hub proteins are structural and/or cellular-matrix proteins (Table S2).

In SYSY-APP$_{Sw}$ cells, we had shown that hub connectors — proteins with few direct interacting partners, which link higher-degree hub proteins that are not otherwise connected — are especially influential in the aggregate contactomes.[10] The present analysis extends this observation to the human AD amyloid contactome. In AD hippocampal Aβ aggregates, there were 195 highly influential hub connectors, which include PGAM1, SQSTM1, CYTB, CRYM, several RAB proteins, and 14-3-3T. Complete list of predicted AD hub connectors are provided as Table S3.

Since phosphorylations play a critical role in modulating protein aggregation,[3,5,7,10] we analyzed phosphorylation status for sarcosyl-insoluble aggregate proteins purified after Aβ pull-down from AD and AMC tissue. We found only 10 out of 66 proteins (15%) with sites that are

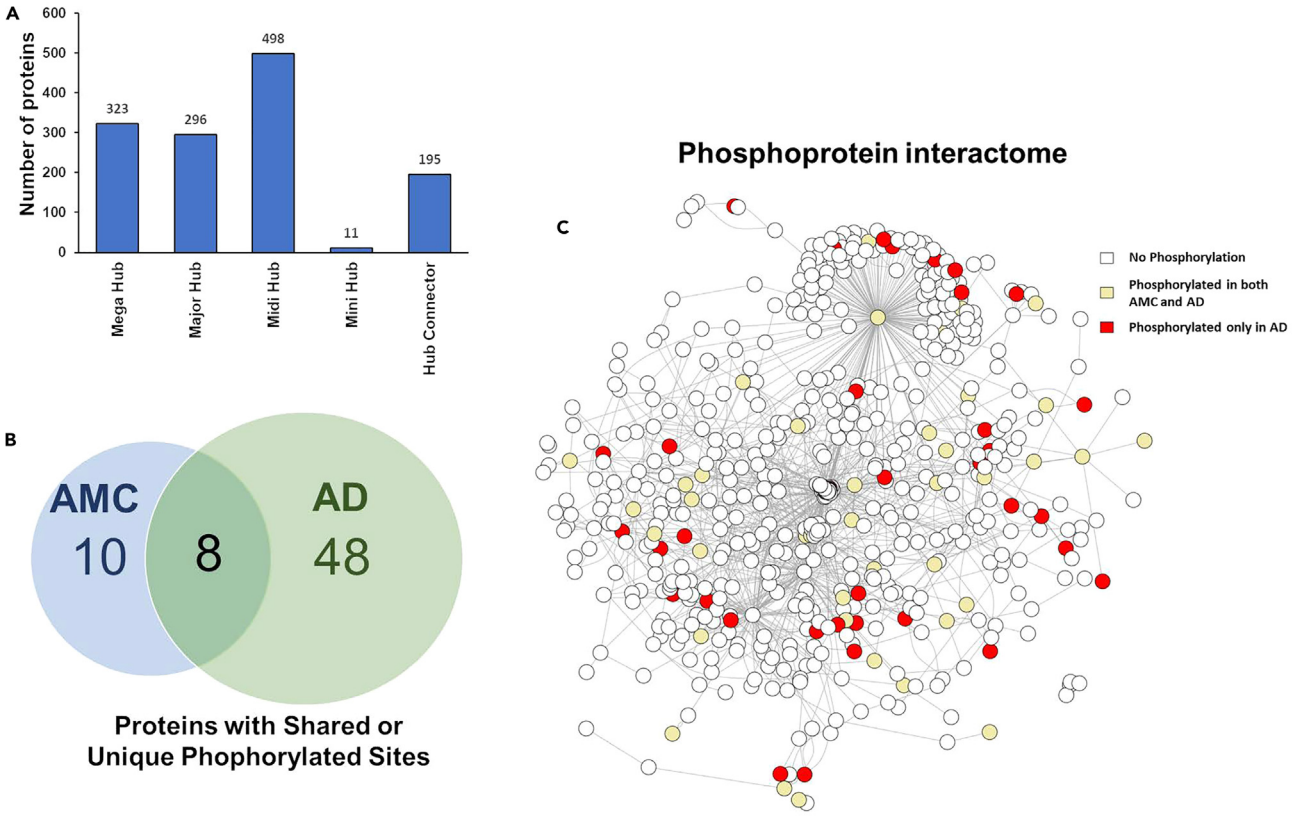

Figure 2. The AD interactome reveals hub and hub-connector proteins

(A) Hub proteins in the AD insoluble-aggregate interactome were categorized, based on the number of interacting partners (degree), into classes ranging from mega-to mini-hubs; "hub connectors" have low degree, but connect hubs that are not otherwise linked.

(B) Venn diagram showing that phosphorylations unique to AD are almost 5 times more abundant than AMC-specific sites in insoluble amyloid aggregates.

(C) Graph network depiction of phosphorylated proteins inferred from proteomic data, representing three categories: absence of phosphorylation (white), phosphorylated in both AMC and AD (yellow), and phosphorylated only in AD aggregates (red). Sites are deemed fully phosphorylated if that PTM comprises >99% of proteomic reads; whereas sites are considered "unphosphorylated" if they carry <20% phosphorylation.

uniquely phosphorylated in AMC aggregates, in contrast to 43 proteins (65%) with sites that are phosphorylated only in AD brain amyloid (Figure 2B). A further 8 proteins are modified by shared site phosphorylations in both AD and AMC aggregates, although not always identically. AD-specific phosphorylations are listed in Table S4, demonstrating the potential diagnostic value of identifying differential PTMs in protein aggregates. Figure 2C illustrates the abundance and pervasiveness of phosphoproteins in the AD-aggregate contactomes. Hubs with AD-specific phosphorylation are colored red, while those shared by AD and AMC are highlighted in yellow.

Mitochondrial and cytoplasmic proteins are enriched in the Alzheimer's disease amyloid contactome

In a previous study comparing the protein compositions of AD vs. AMC aggregates, meta-analysis of the most differentially abundant proteins implicated acetylation, phosphorylation, and oxidation as GO (Gene Ontology) or pathway annotation terms highly and significantly over-represented among AD-aggregate proteins.[7] In the present aggregate-contactome analysis, we identified over 1300 aggregate proteins markedly enriched in 3 out of 3 AD brain samples relative to AMC. Functional-annotation enrichment analysis of these proteins revealed some interesting features. First, we partitioned proteins based on the associated subcellular location. Mitochondrial and cytoplasmic proteins emerge as the cell compartments most highly represented in the aggregate interactome (Figure 3A). More than 20% of the AD aggregate contactome comprises mitochondrial proteins, while over 40% are cytoplasmic. By parsing the AD mitochondrial contactome for disease associations, we revealed enrichment for multiple neurodegenerative diseases, including Parkinson's, Huntington's, and Alzheimer's diseases, as well as prion disease and spinocerebellar ataxia (Figure 3B). Other enriched disease terms were diabetic cardiomyopathy and chemically induced cancers. Mitochondrial proteins in AD aggregates have over 1.6-fold higher degree (number of interacting proteins) than those in AMC contactomes (Figure 3C).

We performed a parallel GO/pathway analysis for the disease association of cytoplasmic proteins identified in the AD aggregate contactome, again revealing significant enrichment for neurodegenerative diseases that include Alzheimer's and Parkinson's diseases, ALS, and prion disease (Figure 3D). Cytoplasmic proteins were also enriched for the insulin and oxytocin signaling pathways, and a variety of infections

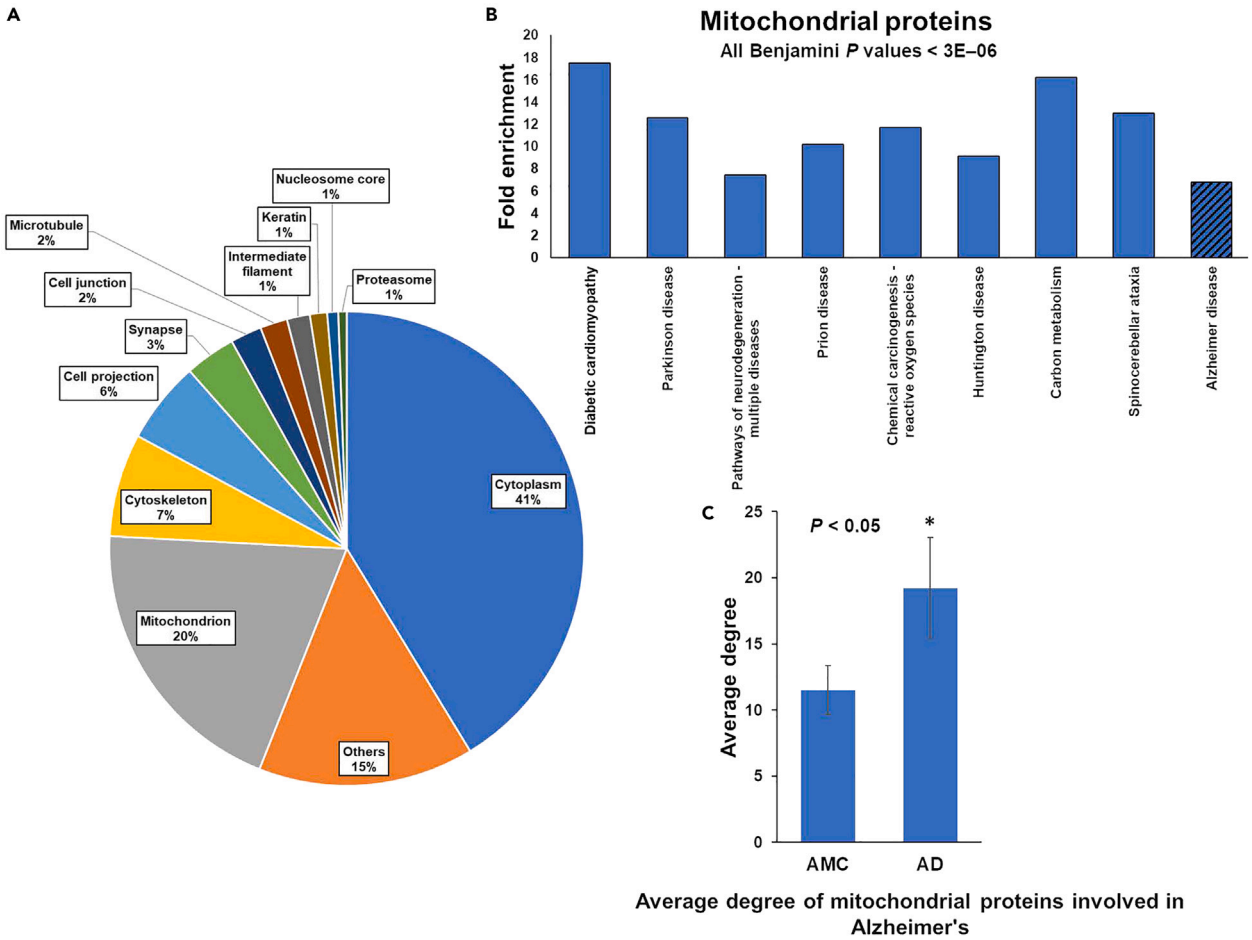
A
Nucleosome core 1%
Keratin 1%
Microtubule 2%
Intermediate filament 1%
Cell junction 2%
Proteasome 1%
Synapse 3%
Cell projection 6%
Cytoplasm 41%
Cytoskeleton 7%
Mitochondrion 20%
Others 15%
B
Mitochondrial proteins
All Benjamini P values < 3E–06
Fold enrichment
Diabetic cardiomyopathy
Parkinson disease
Pathways of neurodegeneration - multiple diseases
Prion disease
Chemical carcinogenesis - reactive oxygen species
Huntington disease
Carbon metabolism
Spinocerebellar ataxia
Alzheimer disease
C
P < 0.05
*
Average degree
AMC
AD
Average degree of mitochondrial proteins involved in Alzheimer's
D
Cytoplasmic proteins
All Benjamini P values < 2E–7
Fold enrichment
Salmonella infection
Pathways of neurodegeneration - multiple diseases
Pathogenic Escherichia coli infection
Gap junction
Regulation of actin cytoskeleton
Endocytosis
Amyotrophic lateral sclerosis
Long-term potentiation
Tight junction
Coronavirus disease - COVID-19
Parkinson disease
Proteoglycans in cancer
Focal adhesion
Prion disease
Oxytocin signaling pathway
Insulin signaling pathway
Ribosome
Alzheimer disease
Adherens junction
Yersinia infection
E
P < 0.05
*
Average degree
AMC
AD

Figure 3. Gene Ontology meta-analysis implicates mitochondrial and cytoplasmic proteins as the principle AD annotations

(A) Pie chart representing the composition of aggregate proteins, based on their cellular component.

(B) Bar chart showing mitochondrial proteins identified in AD aggregates with >2-fold enrichment for disease-pathway annotations and Benjamini-adjusted p value < 3E − 6 for annotation enrichment in DAVID 2022 (https://david.ncifcrf.gov/home.jsp).

(C) Average number of interacting partners (degree) for mitochondrial proteins retrieved from aggregates.

(D) Bar chart showing cytoplasmic proteins recovered from AD aggregates with >2-fold enrichment for disease-pathway annotations and Benjamini-adjusted p values <2E − 7 for annotation-term enrichment in DAVID 2022.

(E) Average degree (number of interacting partners) of cytoplasmic proteins retrieved from aggregates.

(C and E) In these panels, each individual tissue sample is treated as a single point, and significance is assessed by 2-tailed heteroscedastic *t* tests.

(salmonella, *E. coli*, COVID19), suggesting impacts on health and immunity (Figure 3D). Consistent with data for mitochondrial proteins, aggregate-associated cytoplasmic proteins show an increase of over 1.8-fold in degree (interacting partners) in AD relative to AMC (Figure 3E).

Neural network analysis predicts node influence in Alzheimer's disease-like aggregation

The AD aggregate interactome comprises >1,300 proteins, participating in >47,000 protein-protein interactions (Figure 1D). To ascertain which proteins or interactions contribute the most to aggregate formation and stability, we assessed RNAi knockdowns targeting aggregate proteins for rescue of chemotaxis failure in a *C. elegans* model of AD-like amyloidosis. These empirical wet-lab data supplied inputs to train a neural-network (NN) algorithm in R (Orange), which then predicted the influence of each protein in stabilizing aggregates based on their contactome structure.[10] Knockdown (KD) influence predictions were highly correlated ($R = 0.9$; $R^2 = 0.8$) with empirical KD influence in a validation set of previously measured RNAi rescues (Figure 4A). We then predicted KD-influence scores for 1314 proteins (nodes) identified in the AD-specific interactome for Aβ-pulldown aggregates. Graphical visualization of the resulting AD interactome, showing KD-influence scores predicted by the trained neural network, allows us to emphasize differentially influential proteins that appear to play highly leveraged roles in AD aggregate growth and/or stability (Figure 4B, orange and red nodes).

The most influential proteins, represented by orange and red nodes, appear with a wide range of degrees, i.e., varying numbers of interacting partners. The ratio of predicted influence scores, AD/AMC, implicates a subset of aggregate proteins (red hubs in Figure 4B) that are especially influential in AD aggregation — e.g., Aβ peptide (and the parent APP protein); CAND1 (Cullin-associated NEDD8-dissociated protein 1); eEF2 (eukaryote Elongation Factor 2); GFAP (Glial Fibrillary Acidic Protein); 14-3-3E (epsilon); PERI (peripherin); RAB30 (Ras-related protein Rab-30); CH10 (mitochondrial heat shock protein); and ACTN3 (α-actinin 3), each of which has an AD influence predicted to be at least twice that for AMC (Figure 4C). In contrast, some very large structural proteins such as TITIN and SRRM2 were not observed among proteins with very high AD/AMC influence ratios. We then extracted a map of neural-network predicted influential proteins that are direct contacts of Aβ (Figure 4D). This "local contactome" subnetwork reveals several interesting candidate proteins, including CTNA1 (catenin α1) and histone H1-3 (H13), that are predicted to be far more influential in the AD interactome than in AMC, providing a model for understanding accelerated aggregate progression in AD.

Gene ontology analysis identifies disease associations for neural-network-predicted aggregate proteins

Neural network (NN) analysis of aggregation data predicts that certain proteins are especially influential in AD aggregation. To characterize the disease relevance of the top NN-predicted aggregate proteins, we used an annotation-term enrichment meta-analysis of all proteins predicted to be especially influential in AD (AD/AMC influence ratio >1.5) to identify associated diseases, cellular compartments, and diseases that are over-represented. We found significant annotation enrichment for neurodegenerative diseases including Alzheimer's, Huntington's, and Parkinson's diseases, prion disease, and amyotrophic lateral sclerosis (ALS) (Figure 4E), supporting the mechanistic involvement of proteins predicted to stabilize aggregates, in the etiology of diverse neuropathologies.

Knockdown of predicted influential proteins rescues amyloid aggregation in human cells

To empirically assess the validity of neural-network predictions, we selected five of the top protein candidates having node influence ratios (AD/AMC) predicted to be > 1.5: PRKDC, PERI, CTNA2, SPTB1, and ANK3. Individual knockdowns of each of these target proteins by siRNA constructs (Table S5) conferred significant protection against amyloid-like aggregation in SY5Y-APP_{Sw} cells relative to controls (Figure 5), with no visible cytotoxicity (based on the detachment of $DAPI^+$ cells). We infer from this that the observed reduction in Thioflavin T fluorescence reflects lower aggregate formation or stability. Among these aggregate components, KD of *Ank3* and *Peri* genes conferred the greatest protection against aggregation: ∼3.7-fold and ∼2.8-fold, respectively, exceeding their NN-predicted AD/AMC influence ratios of 2.1. Moreover, the predicted AD/AMC influence ratio for CTNA2 was 1.75, very close to the 1.8-fold reduction in thioflavin-positive aggregates observed in SY5Y-APP_{Sw} cells upon transfection with *Ctna2* siRNA. These results collectively support the conclusion that NN-predicted influential proteins such as PERI, ANK3, CTNA2, and SPTB1 are especially important for AD-associated aggregation.

Knockdown of aggregation-prone mitochondrial proteins improves *C. elegans* chemotaxis

Gene ontology prediction showed that proteins in AD aggregates are especially enriched for two cellular compartments, mitochondria and cytoplasm. Previous studies have noted mitochondrial dysfunction in Alzheimer's disease brains.[7] We sought to analyze the importance of

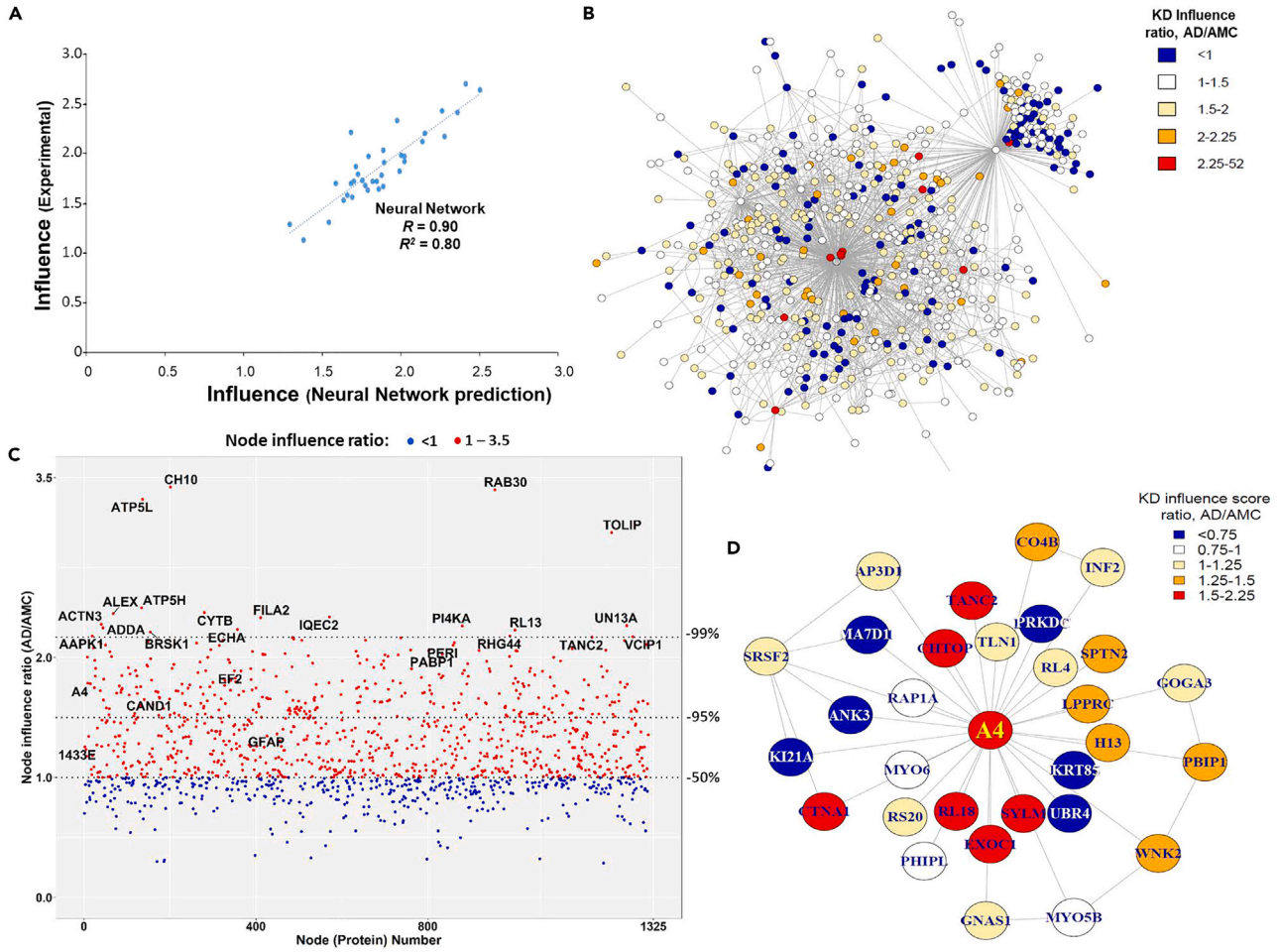
A
Influence (Experimental)
Influence (Neural Network prediction)
Neural Network
R = 0.90
R² = 0.80
B
KD Influence ratio, AD/AMC
<1
1-1.5
1.5-2
2-2.25
2.25-52
C
Node influence ratio: <1 1 – 3.5
Node influence ratio (AD/AMC)
Node (Protein) Number
-99%
-95%
-50%
CH10
RAB30
ATP5L
TOLIP
ALEX
ATP5H
ACTN3
ADDA
CYTB
FILA2
IQEC2
PI4KA
RL13
UN13A
AAPK1
BRSK1
ECHA
PERI
PABP1
RHG44
TANC2
VCIP1
A4
EF2
CAND1
GFAP
1433E
D
KD influence score ratio, AD/AMC
<0.75
0.75-1
1-1.25
1.25-1.5
1.5-2.25
CO4B
AP3D1
INF2
TANC2
PRKDC
MA7D1
CHTOP
TLN1
SRSF2
SPTN2
RL4
GOGA3
RAP1A
LPPRC
ANK3
A4
H13
KI21A
MYO6
KRT85
PBIP1
CTNA1
RS20
RL18
SYLM
UBR4
EXOC1
PHIP1
WNK2
GNAS1
MYO5B
E
NN-predicted influential proteins: disease relevance (DAVID)
All Benjamini P values < 5.1E-7
Fold enrichment
Parkinson disease
Prion disease
Huntington disease
Pathways of neurodegeneration
Alzheimer disease
Diabetic cardiomyopathy
Dopaminergic synapse
Gap junction
Amyotrophic lateral sclerosis

Figure 4. Neural-network prediction of influential proteins in the AD β-amyloid interactome

(A) Correlation between experimentally observed impact of RNAi knockdown (KD) on total aggregate (amyloid) burden in SH-SY5Y-APP$_{Sw}$ cells, and the influence of node removal based on neural network (NN) predictions after training.

(B) Graph model representation of the SY5Y-APP$_{Sw}$ cell contactome, showing AD/AMC ratios of NN-predicted influence. As in Figure 1, orange and red nodes indicate proteins with the highest AD/AMC influence ratios (see key resources table).

(C) Dot-plot representation of AD/AMC ratios of NN-predicted influence scores for 1325 proteins more abundant in AD than AMC aggregates.

(D) Aβ direct (first-degree) interaction partners in AD insoluble aggregates, extracted from the contactome in panel **b**, showing NN-predicted influence ratios (see key resources table).

(E) Bar chart representing fold-enrichment for disease pathway terms annotating NN-predicted influential proteins from AD aggregates, having AD/AMC influence ratio >2.0.

aggregation-prone mitochondrial proteins that were enriched in AD aggregates. Gene knockdowns of mitochondrial proteins, that differ markedly in predicted influence between AMC and AD aggregates, were assessed in a *C. elegans* strain with the neuronal expression of human Aβ_{1-42}. These KDs reduced the levels of amyloid-like aggregates, which impaired chemotaxis progressively with age.[7] Specifically, 4 of 8 knockdowns of *C. elegans* orthologs of human genes encoding mitochondrial proteins enriched in AD aggregates (*rmd-3, odp-2, pgam-5,* and *nduf-2.2*) significantly protect against chemotaxis decline in worms expressing Aβ_{42} in neurons (Figure 5C). This illustrates the importance of mitochondrial dysregulation and possible roles of aggregation-prone mitochondrial proteins in AD pathogenesis.

DISCUSSION

In this study, utilizing "click chemistry" to crosslink proximal proteins within aggregates, we constructed an aggregate-specific protein-contact network from AD-patient and control brains.

Through proteomic analyses of AD and AMC aggregates, we previously identified proteins that co-aggregate with Aβ in extracellular plaque, or with hyperphosphorylated tau in neurofibrillary tangles.[7] Such proteomic analysis revealed the true complexity of AD aggregates in general. Knockdowns achieved by the siRNA transfection of SY5Y-APP$_{Sw}$ neuroblastoma cells allowed us to suppress the expression of individual proteins that are significantly and specifically enriched in AD aggregates, confirming pro-aggregation roles for many of the implicated proteins — including GFAP, eEF2, 14-3-3 family members, and SERF2.[5,6,9,10] These results imply that the aggregation of many proteins is nonrandom, favoring specific protein-protein interfaces (PPI) for adhesion.[2,5–10,21] However, the interfaces through which proteins interact within aggregates were not previously known. In the present study, we used the same protein-crosslinking technique that we had previously established in a simple neuroblastoma cell model[10] to derive the AD contactome (non-functional interactome) as a consensus amyloid-plaque structure differentiating AD from AMC hippocampi. The complex interaction network for AD plaque revealed hub proteins with greater abundance and interaction complexity than the same hubs in AMC aggregates, features that are expected to contribute to the insoluble-aggregate burden in AD. Most protein-protein interactions observed in AD aggregates were not found at all in AMC; e.g., the interaction of GFAP with dynactin-1 (DCTN1) is unique to AD. Interestingly, both GFAP and DCTN1 were enriched in AD serum relative to AMC.[22] Although Dey et al. did not isolate aggregates, their serum proteomics would have included them, and thus are consistent with our finding that these proteins occur in AD aggregates at elevated levels, and suggest the possibility that these proteins may have leaked into cerebrospinal fluid, and thence into the bloodstream, from dead or dying brain tissue.

The observation in AD brain amyloid of hubs with far more interacting partners per node (higher degree) suggests that such proteins may support the growth or stability of aggregates. Although we previously demonstrated that knockdown of proteins that are relatively enriched in AD aggregates confers protection against aggregation in multiple model systems,[2,6,10] our current AD-specific interactome data allow hub proteins to be ranked by their AD/AMC degree ratio, which is likely to contribute to the aggregate abatement we observed after KD of either partner.

We previously reported that numerous proteins identified in AD aggregates are differentially phosphorylated. We surmised that AD-specific phosphorylations may predispose these proteins to misfolding and aggregation,[10] and may recruit other proteins to conglomerate in insoluble aggregates. Our current proteomics data identified 66 proteins that are phosphorylated only in AD but unmodified in AMC aggregates. This is likely due to previously demonstrated, AD-specific elevation of the implicated kinases, including MAPK-p38, GSK3β, and PKA.[23–27] Studies have documented that inhibiting the activity of these kinases lowered aggregation of critical proteins, including tau, GFAP, and α-synuclein, demonstrating the role of phosphorylation in AD pathology.[5,26,28] Griffin et al. (1989) reported that neuroinflammation, and IL1β in particular, drive the synthesis and activation of several AD-elevated kinases that underlie tau hyperphosphorylation.[29] Our identification of uniquely phosphorylated proteins in AD aggregates implicates new protein and PPI targets for therapeutically opposing PTM events that drive aggregation.

Organelles, including mitochondria and endoplasmic reticulum, have long been implicated in AD pathogenesis.[30,31] Gene ontology meta-analysis of top-ranked aggregate proteins (as predicted by NN analysis of network structure) revealed that ~20% of them are mitochondrial. This suggests two possibilities: (***i.***) Due to aging and/or stress, including Aβ stress, mitochondria form insoluble aggregates, leading to mitochondrial dysfunction. (***ii.***) Accumulation of Aβ peptide in mitochondria is responsible for mitochondrial dysfunction/disintegration, resulting in leakage of mitochondrial proteins into the cytosol, where they coalesce with other aggregation-prone proteins. Meta-analysis of these AD-enriched mitochondrial proteins implicates pathways specific for diverse neurodegenerative diseases, strongly implying that mitochondrial proteins play a highly leveraged role in disease pathology. We are currently pursuing this possibility by analysis of aggregates isolated directly from mitochondria of AD vs. AMC brain tissue. This is important because we believe that both intra- and extra-cellular aggregates are crucial

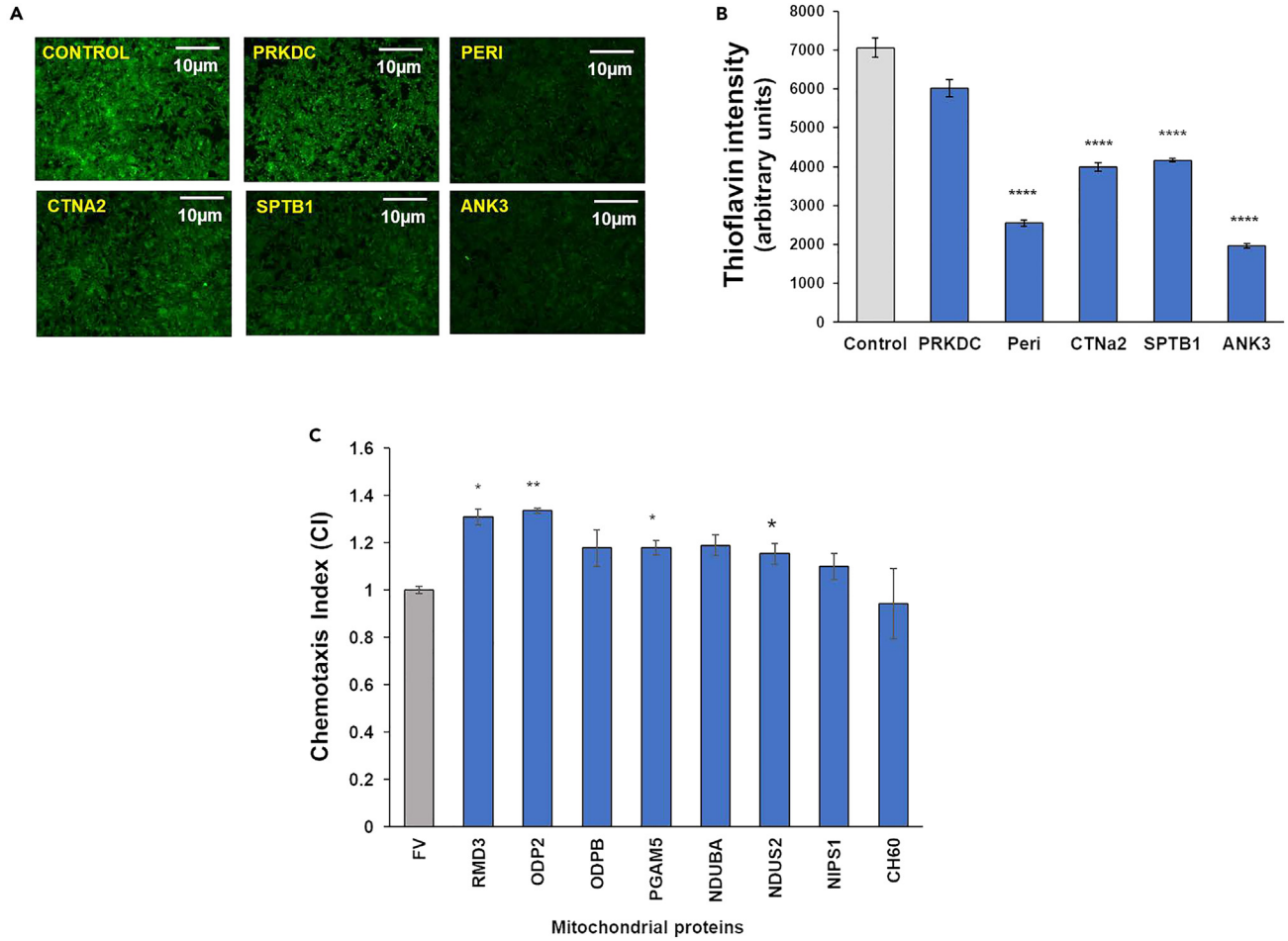

Figure 5. Aggregate burden in SY5Y-APP$_{Sw}$ cells and a *C elegans* model of neuronal amyloidosis is reduced after exposure to siRNAs targeting predicted highly influential proteins

(A) Thioflavin-T staining of amyloid-like aggregates in SY5Y-APP$_{Sw}$ cells treated with siRNAs targeting the indicated proteins, or with a random-sequence siRNA construct (control) to assess nonspecific effects of the transfection protocol.

(B) Histogram shows thioflavin-T fluorescence of amyloid-like aggregates per cell in controls vs. siRNA-treated cells. Error bars indicate ±SEM. ****$p < 1E{-}40$.

(C) We tested 8 influential mitochondrial proteins implicated in AD aggregates, by RNAi knockdown in a *C. elegans* AD model expressing A$\beta_{1\text{-}42}$ in neurons and consequently displaying impaired chemotaxis. Of these, 4 (50%) showed significant rescue of chemotaxis, in each case comparing three biological repeats by 1-tailed paired *t*-tests (*$p < 0.05$; **$p < 0.005$). At least 2 out of 3 biological assays for each KD target, taken individually, showed significant rescue relative to controls (no KD) by chi-squared test, at $p \leq 0.01$.

determinants in AD pathology, in that one contributes to the other, forming a vicious cycle that ultimately leads to neuropathology. Intracellular aggregates, especially aggregates formed in the organelles such as mitochondria, damages those organelles and may lead to cell death. In many instances, Aβ peptide is known to exacerbate intra-cellular/organelle aggregation, suggesting that intra- and extra-cellular aggregation are not independent of one another.[32]

GO analysis of AD-enriched aggregate proteins also identified pathways related to infectious agents, including *Salmonella* and *E. coli* bacteria and SARS-CoV2 virus. This is interesting because the risk of dementia was reported to be higher in patients after Herpes Simplex Virus (HSV) infection, than in non-HSV controls or HSV-positive patients who received anti-herpetic drugs (e.g., Acyclovir, Famciclovir, Ganciclovir, Valciclovir, or Valganciclovir).[33,34] Neuroinflammation is a critical component of AD pathology, and infections increase a variety of neuroinflammatory cytokines, and IL-1β in particular.[29,35–38] Increased IL-1β stimulates the production of sAPPα and eventually Aβ, leading to plaque formation. On the other hand, AD brains are more vulnerable to diverse infections, including *E. coli*, which are often associated with cognitive decline.[39] Aggregate proteomics revealed that several constituent proteins, including structural proteins (e.g., actin, dynactin, and tubulins) and regulatory proteins (e.g., ATP-ribosylation factors and small GTP-binding proteins), are involved in pathways related to infection, suggesting common mechanisms linking immune activation to AD etiology.

Furthermore, our use of neural-network algorithms to predict the relative influence of nodes in the aggregate interactome identified several proteins that are critical to aggregate burden. Recruitment of proteins into aggregates is non-random,[10] and due to the complex

3D structure of the aggregate "contactomes," the component proteins vary widely in their impact on aggregate growth and stability.[10] We used a machine-learning/neural-network approach to prioritize hubs and PPIs as potential therapeutic targets. Neural-network predictions correlated extremely well ($R = 0.9$) with experimental values in test datasets derived from gene knockdowns in a *C. elegans* model of AD, allowing us to identify key amyloid-interactome proteins (e.g., APP, GFAP, eEF2, CAND1, TENS1, MAP1A, and FLNC) predicted to be the most influential contributors to aggregate burden; these predictions were then validated by gene knockdowns in *C. elegans*.

The static interactome (contactome) of AD-specific aggregates described here delineates a complex web of aggregate-specific PPIs that mediate aggregate growth and stability. A detailed understanding of aggregate architecture implicates key hub proteins and PPIs. Targeting such influential proteins with small molecules can reduce the complexity of aggregates and/or halt further aggregate growth. For example, in our previous work, we found GFAP to be an influential protein that plays a crucial role in aggregate growth and complexity. Target-based *in silico* screening of small-molecule structural libraries predicted several that specifically target GFAP; the best candidate was validated in several AD-model systems wherein we observed highly significant reductions in aggregate burden.[5,21] The approach, strategies, and more importantly the influential proteins, described here can be generalized to many other neurodegenerative diseases that feature age-associated protein aggregation as hallmarks.

Limitations of the study

(1) Recovery of Aβ-specific aggregates from brain samples depends on antibody specificity and avidity for its target. We validated the antibody employed here for specificity based on binding to protein of the expected electrophoretic mobility.[7] Due to differences in avidity among antibodies, no comparisons could be made between recoveries of different proteins; thus, relative proteomic spectral counts ("hits") are used only to compare AD vs. AMC yields of the same protein.

(2) Quantitation of cross-linked peptides from aggregates depends on the extent to which trypsin can digest intra-aggregate proteins. We assessed whether protease digestion can progressively degrade aggregates using AD-model systems, including SY5Y-APP$_{Sw}$ human neural cells and *C. elegans*.[10] Based on material failing enter a polyacrylamide electrophoretic gel, we estimate that trypsin digests $\geq$94% of sarcosyl-insoluble aggregates from AD hippocampus. Such material was excluded from analyses under our current protocol. Yields of each crosslinked-protein were only compared between AD and AMC.

(3) Identification of cross-linked peptide pairs depends on both proteins being included in a reference list of aggregate proteins and their post-translational modifications (PTMs), identified in aggregates isolated without crosslinking. Proteins and PTMs not detected in reference aggregates will not be registered by the software. Identification of cross-linked peptides requires high-resolution outputs from mass spectrometry, and may exceed the local computational capability for large reference lists. No such limitation was encountered in the present study.

STAR★METHODS

Detailed methods are provided in the online version of this paper and include the following:

- KEY RESOURCES TABLE
- RESOURCE AVAILABILITY
  - Lead contact
  - Materials availability
  - Data and code availability
- EXPERIMENTAL MODEL AND STUDY PARTICIPANT DETAILS
  - Institutional approval of ethical procedures
- METHOD DETAILS
  - Purification of Aβ-specific sarcosyl-insoluble aggregates
  - Chemical cross-linking of insoluble aggregates
  - Graph modeling of protein-protein interaction (PPI) networks
  - Neural-network analyses
  - siRNA knockdowns and thioflavin-T staining in SY5Y-APPsw cells
  - RNAi knockdown and chemotaxis assay in a *C. Elegans* AD model
  - Thioflavin-T staining of amyloid-like aggregates in SY5Y-APP$_{Sw}$ cells
- QUANTIFICATION AND STATISTICAL ANALYSIS

SUPPLEMENTAL INFORMATION

Supplemental information can be found online at https://doi.org/10.1016/j.isci.2023.108745.

ACKNOWLEDGMENTS

This work was supported by funding from the following grants: 1R01 AG062254 to S.A. and R.J.S.R., and Program Project grant 2P01AG012411-17A1 (W.S.T. Griffin, P.I.), both from the U.S. National Institute on Aging; Merit Review Award I01 BX001655 and Senior

Research Career Scientist Award IK6 BX004851 to R.J.S.R. from the U.S. Dept. of Veteran Affairs; and an award to M.B. from the Inglewood Scholars Program. We thank Dr. Sue T. Griffin for kindly providing frozen human brain samples from the Alzheimer's Disease Brain Bank, which she maintains at the University of Arkansas for Medical Sciences, Institute on Aging.

DECLARATION OF INTERESTS

The authors declare no competing interests.

Received: August 15, 2023
Revised: November 15, 2023
Accepted: December 12, 2023
Published: December 18, 2023

REFERENCES

1. Zhang, X., Fu, Z., Meng, L., He, M., and Zhang, Z. (2018). The Early Events That Initiate beta-Amyloid Aggregation in Alzheimer's Disease. Front. Aging Neurosci. *10*, 359.
2. Ayyadevara, S., Balasubramaniam, M., Gao, Y., Yu, L.R., Alla, R., and Shmookler Reis, R. (2015). Proteins in aggregates functionally impact multiple neurodegenerative disease models by forming proteasome-blocking complexes. Aging Cell *14*, 35–48.
3. Ayyadevara, S., Balasubramaniam, M., Johnson, J., Alla, R., Mackintosh, S.G., and Shmookler Reis, R.J. (2016). PIP3-binding proteins promote age-dependent protein aggregation and limit survival in C. elegans. Oncotarget *7*, 48870–48886.
4. Ayyadevara, S., Balasubramaniam, M., Suri, P., Mackintosh, S.G., Tackett, A.J., Sullivan, D.H., Shmookler Reis, R.J., and Dennis, R.A. (2016). Proteins that accumulate with age in human skeletal-muscle aggregates contribute to declines in muscle mass and function in Caenorhabditis elegans. Aging (Albany NY) *8*, 3486–3497.
5. Ganne, A., Balasubramaniam, M., Griffin, W.S.T., Shmookler Reis, R.J., and Ayyadevara, S. (2022). Glial Fibrillary Acidic Protein: A Biomarker and Drug Target for Alzheimer's Disease. Pharmaceutics *14*, 1354.
6. Balasubramaniam, M., Ayyadevara, S., and Shmookler Reis, R.J. (2018). Structural insights into pro-aggregation effects of C. elegans CRAM-1 and its human ortholog SERF2. Sci. Rep. *8*, 14891.
7. Ayyadevara, S., Balasubramaniam, M., Parcon, P.A., Barger, S.W., Griffin, W.S.T., Alla, R., Tackett, A.J., Mackintosh, S.G., Petricoin, E., Zhou, W., and Shmookler Reis, R.J. (2016). Proteins that mediate protein aggregation and cytotoxicity distinguish Alzheimer's hippocampus from normal controls. Aging Cell *15*, 924–939.
8. Ayyadevara, S., Ganne, A., Balasubramaniam, M., and Shmookler Reis, R.J. (2022). Intrinsically disordered proteins identified in the aggregate proteome serve as biomarkers of neurodegeneration. Metab. Brain Dis. *37*, 147–152.
9. Ganne, A., Balasubramaniam, M., Mainali, N., Atluri, P., Shmookler Reis, R.J., and Ayyadevara, S. (2022). Physiological Consequences of Targeting 14-3-3 and Its Interacting Partners in Neurodegenerative Diseases. Int. J. Mol. Sci. *23*, 15457.
10. Balasubramaniam, M., Ayyadevara, S., Ganne, A., Kakraba, S., Penthala, N.R., Du, X., Crooks, P.A., Griffin, S.T., and Shmookler Reis, R.J. (2019). Aggregate Interactome Based on Protein Cross-linking Interfaces Predicts Drug Targets to Limit Aggregation in Neurodegenerative Diseases. iScience *20*, 248–264.
11. Ayyadevara, S., Balasubramaniam, M., Kakraba, S., Alla, R., Mehta, J.L., and Shmookler Reis, R.J. (2017). Aspirin-Mediated Acetylation Protects Against Multiple Neurodegenerative Pathologies by Impeding Protein Aggregation. Antioxidants Redox Signal. *27*, 1383–1396.
12. Stark, L.A., Reid, K., Sansom, O.J., Din, F.V., Guichard, S., Mayer, I., Jodrell, D.I., Clarke, A.R., and Dunlop, M.G. (2007). Aspirin activates the NF-kappaB signalling pathway and induces apoptosis in intestinal neoplasia in two in vivo models of human colorectal cancer. Carcinogenesis *28*, 968–976.
13. Blair, L.J., Sabbagh, J.J., and Dickey, C.A. (2014). Targeting Hsp90 and its co-chaperones to treat Alzheimer's disease. Expert Opin. Ther. Targets *18*, 1219–1232.
14. David, D.C., Ollikainen, N., Trinidad, J.C., Cary, M.P., Burlingame, A.L., and Kenyon, C. (2010). Widespread protein aggregation as an inherent part of aging in C. elegans. PLoS Biol. *8*, e1000450.
15. Du, X., Chowdhury, S.M., Manes, N.P., Wu, S., Mayer, M.U., Adkins, J.N., Anderson, G.A., and Smith, R.D. (2011). Xlink-identifier: an automated data analysis platform for confident identifications of chemically cross-linked peptides using tandem mass spectrometry. J. Proteome Res. *10*, 923–931.
16. Jacomy, M., Venturini, T., Heymann, S., and Bastian, M. (2014). ForceAtlas2, a continuous graph layout algorithm for handy network visualization designed for the Gephi software. PLoS One *9*, e98679.
17. Pedersini, C.A., Guàrdia-Olmos, J., Montalà-Flaquer, M., Cardobi, N., Sanchez-Lopez, J., Parisi, G., Savazzi, S., and Marzi, C.A. (2020). Functional interactions in patients with hemianopia: A graph theory-based connectivity study of resting fMRI signal. PLoS One *15*, e0226816.
18. Mondragón, R.J. (2020). Estimating degree-degree correlation and network cores from the connectivity of high-degree nodes in complex networks. Sci. Rep. *10*, 5668.
19. Labbadia, J., and Morimoto, R.I. (2015). The biology of proteostasis in aging and disease. Annu. Rev. Biochem. *84*, 435–464.
20. Ayyadevara, S., Mercanti, F., Wang, X., Mackintosh, S.G., Tackett, A.J., Prayaga, S.V.S., Romeo, F., Shmookler Reis, R.J., and Mehta, J.L. (2016). Age- and Hypertension-Associated Protein Aggregates in Mouse Heart Have Similar Proteomic Profiles. Hypertension *67*, 1006–1013.
21. Kakraba, S., Ayyadevara, S., Penthala, N.R., Balasubramaniam, M., Ganne, A., Liu, L., Alla, R., Bommagani, S.B., Barger, S.W., Griffin, W.S.T., et al. (2019). A Novel Microtubule-Binding Drug Attenuates and Reverses Protein Aggregation in Animal Models of Alzheimer's Disease. Front. Mol. Neurosci. *12*, 310.
22. Dey, K.K., Wang, H., Niu, M., Bai, B., Wang, X., Li, Y., Cho, J.H., Tan, H., Mishra, A., High, A.A., et al. (2019). Deep undepleted human serum proteome profiling toward biomarker discovery for Alzheimer's disease. Clin. Proteonomics *16*, 16.
23. Sun, A., Liu, M., Nguyen, X.V., and Bing, G. (2003). P38 MAP kinase is activated at early stages in Alzheimer's disease brain. Exp. Neurol. *183*, 394–405.
24. Gee, M.S., Son, S.H., Jeon, S.H., Do, J., Kim, N., Ju, Y.J., Lee, S.J., Chung, E.K., Inn, K.S., Kim, N.J., and Lee, J.K. (2020). A selective p38alpha/beta MAPK inhibitor alleviates neuropathology and cognitive impairment, and modulates microglia function in 5XFAD mouse. Alzheimers Res. Ther. *12*, 45.
25. Lauretti, E., Dincer, O., and Praticò, D. (2020). Glycogen synthase kinase-3 signaling in Alzheimer's disease. Biochim. Biophys. Acta Mol. Cell Res. *1867*, 118664.
26. Balasubramaniam, M., Mainali, N., Bowroju, S.K., Atluri, P., Penthala, N.R., Ayyadevera, S., Crooks, P.A., and Shmookler Reis, R.J. (2020). Structural modeling of GSK3beta implicates the inactive (DFG-out) conformation as the target bound by TDZD analogs. Sci. Rep. *10*, 18326.
27. Carlyle, B.C., Nairn, A.C., Wang, M., Yang, Y., Jin, L.E., Simen, A.A., Ramos, B.P., Bordner, K.A., Craft, G.E., Davies, P., et al. (2014). cAMP-PKA phosphorylation of tau confers risk for degeneration in aging association cortex. Proc. Natl. Acad. Sci. USA *111*, 5036–5041.
28. Lee, J.K., and Kim, N.J. (2017). Recent Advances in the Inhibition of p38 MAPK as a Potential Strategy for the Treatment of Alzheimer's Disease. Molecules *22*, 1287.
29. Griffin, W.S., Stanley, L.C., Ling, C., White, L., MacLeod, V., Perrot, L.J., White, C.L., 3rd, and Araoz, C. (1989). Brain interleukin 1 and S-100 immunoreactivity are elevated in Down syndrome and Alzheimer disease. Proc. Natl. Acad. Sci. USA *86*, 7611–7615.
30. Li, Z., Cao, Y., Pei, H., Ma, L., Yang, Y., and Li, H. (2023). The contribution of mitochondria-associated endoplasmic reticulum membranes (MAMs) dysfunction in Alzheimer's disease and the potential

countermeasure. Front. Neurosci. *17*, 1158204.

31. Wang, W., Zhao, F., Ma, X., Perry, G., and Zhu, X. (2020). Mitochondria dysfunction in the pathogenesis of Alzheimer's disease: recent advances. Mol. Neurodegener. *15*, 30.
32. Reddy, P.H., and Beal, M.F. (2008). Amyloid beta, mitochondrial dysfunction and synaptic damage: implications for cognitive decline in aging and Alzheimer's disease. Trends Mol. Med. *14*, 45–53.
33. Tzeng, N.S., Chung, C.H., Lin, F.H., Chiang, C.P., Yeh, C.B., Huang, S.Y., Lu, R.B., Chang, H.A., Kao, Y.C., Yeh, H.W., et al. (2018). Anti-herpetic Medications and Reduced Risk of Dementia in Patients with Herpes Simplex Virus Infections-a Nationwide, Population-Based Cohort Study in Taiwan. Neurotherapeutics *15*, 417–429.
34. Himmelhoch, E., Latham, O., and McDONALD, C.G. (1947). Alzheimer's disease complicated by a terminal salmonella infection. Med. J. Aust. *1*, 701–703.
35. Sheng, J.G., Boop, F.A., Mrak, R.E., and Griffin, W.S. (1994). Increased neuronal beta-amyloid precursor protein expression in human temporal lobe epilepsy: association with interleukin-1 alpha immunoreactivity. J. Neurochem. *63*, 1872–1879.
36. Stanley, L.C., Mrak, R.E., Woody, R.C., Perrot, L.J., Zhang, S., Marshak, D.R., Nelson, S.J., and Griffin, W.S. (1994). Glial cytokines as neuropathogenic factors in HIV infection: pathogenic similarities to Alzheimer's disease. J. Neuropathol. Exp. Neurol. *53*, 231–238.
37. Griffin, W.S., Sheng, J.G., Royston, M.C., Gentleman, S.M., McKenzie, J.E., Graham, D.I., Roberts, G.W., and Mrak, R.E. (1998). Glial-neuronal interactions in Alzheimer's disease: the potential role of a 'cytokine cycle' in disease progression. Brain Pathol. *8*, 65–72.
38. Sheng, J.G., Zhu, S.G., Jones, R.A., Griffin, W.S., and Mrak, R.E. (2000). Interleukin-1 promotes expression and phosphorylation of neurofilament and tau proteins in vivo. Exp. Neurol. *163*, 388–391.
39. Schütze, S., Döpke, A., Kellert, B., Seele, J., Ballüer, M., Bunkowski, S., Kreutzfeldt, M., Brück, W., and Nau, R. (2022). Intracerebral Infection with E. coli Impairs Spatial Learning and Induces Necrosis of Hippocampal Neurons in the Tg2576 Mouse Model of Alzheimer's Disease. J. Alzheimers Dis. Rep. *6*, 101–114.
40. Schneider, C.A., Rasband, W.S., and Eliceiri, K.W. (2012). NIH Image to ImageJ: 25 years of image analysis. Nat. Methods *9*, 671–675.
41. Chowdhury, S.M., Du, X., Tolić, N., Wu, S., Moore, R.J., Mayer, M.U., Smith, R.D., and Adkins, J.N. (2009). Identification of cross-linked peptides after click-based enrichment using sequential collision-induced dissociation and electron transfer dissociation tandem mass spectrometry. Anal. Chem. *81*, 5524–5532.
42. Mousavi, M., and Hellström-Lindahl, E. (2009). Nicotinic receptor agonists and antagonists increase sAPPalpha secretion and decrease Abeta levels in vitro. Neurochem. Int. *54*, 237–244.
43. Link, C.D. (1995). Expression of human beta-amyloid peptide in transgenic Caenorhabditis elegans. Proc. Natl. Acad. Sci. USA *92*, 9368–9372.
44. Dosanjh, L.E., Brown, M.K., Rao, G., Link, C.D., and Luo, Y. (2010). Behavioral phenotyping of a transgenic Caenorhabditis elegans expressing neuronal amyloid-beta. J. Alzheimers Dis. *19*, 681–690.
45. Kamath, R.S., and Ahringer, J. (2003). Genome-wide RNAi screening in Caenorhabditis elegans. Methods *30*, 313–321.
46. Schindelin, J., Arganda-Carreras, I., Frise, E., Kaynig, V., Longair, M., Pietzsch, T., Preibisch, S., Rueden, C., Saalfeld, S., Schmid, B., et al. (2012). Fiji: an open-source platform for biological-image analysis. Nat. Methods *9*, 676–682.

STAR★METHODS

KEY RESOURCES TABLE

REAGENT or RESOURCE	SOURCE	IDENTIFIER
Antibodies		
monoclonal antibody Aβ1–17	Abcam	ab_11132; RRID: AB_297770
Biological samples		
Frozen brain tissue from hippocampus (AMC), N = 3	UAMS brain bank	Not applicable
Frozen brain tissue from hippocampus (AD), N = 3	UAMS brain bank	Not applicable
Chemicals, peptides, and recombinant proteins		
Cross-linking reagents	Balasubramaniam et al. (2019)[10]	Not applicable
Experimental models: Cell lines		
SY5Y-APPsw cell line	Mousavi & Hellström-Lindahl et al.,[14]	Not applicable
Experimental models: Organisms/strains		
C.elegans AD model	CAENORHABDITIS GENETICS CENTER (CGC)	CL2355
Oligonucleotides		
PRKDC	Sigma	SASI_Hs01_00134549
CTNNA2	Sigma	SASI_Hs01_00024061
SPTNB1	Sigma	SASI_Hs01_00083730
ANK3	Sigma	SASI_Hs01_ 00186165
Software and algorithms		
Xlink Identifier	Modified in-house	Du et al., 2011[15]
Orange data mining software	Orange	https://orangedatamining.com/
Fiji-ImageJ	Schneider et al.[40]	https://ImageJ.net/software/fiji/
GePhi graph modeling software	Open Source	https://gephi.org/

RESOURCE AVAILABILITY

Lead contact

Further information and requests for resources and reagents should be directed to and will be fulfilled by the lead contact: Robert J Shmookler Reis (rjsr@uams.edu).

Materials availability

This study did not generate new unique reagents.

Data and code availability

The raw Xlinked data generated in this manuscript, and any additional information required to reanalyze the data reported in this paper is available from the lead contact upon request.

EXPERIMENTAL MODEL AND STUDY PARTICIPANT DETAILS

Institutional approval of ethical procedures

Samples for proteomic analysis were excised from brain tissue archived at −80°C in the UAMS Brain Bank, originating from subjects diagnosed by immunohistochemistry to have Alzheimer's disease (but lacking markers of Parkinson's disease) or age-matched controls (AMCs). Tissues were de-identified, by removal of all identifiers and personal information that could be used to link them to their donors. All experimental procedures described were deemed non-human-subject research by our Institutional Review Board (IRB) under Exemption 4 (U.S. Department of Health and Human Services).

METHOD DETAILS

Purification of Aβ-specific sarcosyl-insoluble aggregates

Detailed methods describing purification of insoluble aggregates from brain tissue were reported previously.[7] Briefly, flash-frozen tissue from AD or AMC brain caudal hippocampus ($N = 3$ per group) was pulverized in a mortar and pestle pre-cooled on dry ice. After a 5-min low-speed centrifugation (2200 x g), supernatant protein was quantified with Bradford reagent (Bio-Rad) and equal protein portions were analyzed. To isolate Aβ-specific aggregates, samples were incubated with DYNAL Protein-G magnetic beads coated with monoclonal antibody raised against a synthetic $A\beta_{1-17}$ peptide (ab11132; Abcam). Bound aggregates were rinsed 3 times, eluted, and brought to 1% v/v sarcosyl, 0.1-M HEPES, 5-mM EDTA, to which was added a cocktail of protease and phosphatase inhibitors (Sigma Aldrich PPC1010). Sarcosyl-insoluble aggregates were pelleted by ultracentrifugation (90 min at 100,000 × g), resuspended in 20-mM phosphate-buffered saline (pH 7.5), and processed for cross-linking.[10]

Chemical cross-linking of insoluble aggregates

A modified cross-linking reagent,[10,41] propargyl amine, was prepared as a stock solution in DMSO and added to insoluble aggregate fractions to achieve a final concentration of 5 μM, and incubated 30 min at 22°C. Cross-linking reactions were quenched with 50-mM Tris-HCl (pH 8.0), and samples were centrifuged 90 min at 100,000 x g at 4°C to remove unbound cross-linker.

Cross-linked aggregates were then incubated in 8-M urea and 122-mM dithiothreitol buffer for 30 min at 37°C. To this reaction mix, 40-mM iodoacetamide was added and incubated 20 min at 22°C in the dark. To the reduced cross-linked sample, 10 units of trypsin (Pierce) was added, and ammonium bicarbonate to 150 mM, for 14 h incubation at 37°C followed by quenching with addition of acetic acid to 3% (v/v).

Trypsin-digested cross-linked peptides are then desalted on a 1-cc C18 column (Sep-Pak, Waters) containing 50 mg resin, and evaporated to dryness (Speed-Vac, ThermoFisher). Samples were then reconstituted in a 10-fold molar excess of biotin crosslinker/azide solution, 0.25-mM TBTA, 250-μM $CuSO_4$, and 5-mM Tris-phosphine (TCEP) buffer, and incubated at 4°C for 2 h. Biotinylated cross-linked peptide pairs were captured on streptavidin-coated magnetic beads as described[10] (ref). Bound cross-linked peptides were eluted in buffer containing 50% (w/v) acetonitrile and 0.4% (v/v) trifluoro-acetic acid, and identified by LC-MS/MS as previously described.

Graph modeling of protein-protein interaction (PPI) networks

Cross-linked peptide pairs were identified and their relative abundances estimated with a modified version of Xlink-Identifier.[10,15] A list of Aβ-specific aggregate proteins, identified previously,[7] was used as a reference database to calculate m/z values for all possible peptide pairs that could arise by cross-linking proteins within aggregates. To reduce the complexity of cross-linking data, only peptide-peptide pairs attaining ≥5 spectral hits per sample were included for further analysis. To reduce false positives, only protein-protein pairs identified in all three individual brain samples were carried forward for further data processing. All data analyses were performed using Linux scripts developed in-house. Results from Xlink-Identifier were first processed by GePhi[16] to calculate network descriptors, including the number of interacting partners (degree) and eigenvector centrality, utilized as independent-variable inputs for NN analysis.

Neural-network analyses

For neural network predictions, we employed our previously trained model,[10] containing experimental data from 36 knockdowns in a *C. elegans* neural-Aβ model. Briefly, NN utilized a multilayer perceptron (MLP) algorithm with back-propagation, implemented within Orange. The NN algorithm had 1 hidden layer with 5100 neurons, and the activation method and solver were set to ReLu and Adam respectively.[10] For training and testing, data were randomly split 70%/30% at each of 100 iterations. The chemotaxis index (normalized as fold change) was predicted and plotted for the full dataset.

siRNA knockdowns and thioflavin-T staining in SY5Y-APPsw cells

To knock down the expression of target genes, human neuroblastoma cell line SH-SY5Y-$APP_{Sw,}$ expressing the "Swedish" familial-AD mutations was maintained as previously described.[6,10,42] Briefly, cells were grown to 70% confluence, trypsinized, and sub-cultured in 96-well plates (at 30,000–40,000 cells/well), supplemented with antibiotic-free Dulbecco's Modified Eagle's Medium (DMEM) containing 10% (v/v) fetal bovine serum (Atlanta Biologicals, GA, USA). After 24 h at 37°C, Lipofectamine 3000 (Invitrogen) was used to transfect cells with a short interfering RNA (siRNA; Sigma Aldrich), targeting each candidate gene of interest, viz., *PRKDC* (SASI_Hs01_00134549), *CTNNA2* (SASI_Hs01_00024061), *SPTNB1* (SASI_Hs01_00083730), and *ANK3* (SASI_Hs01_ 00186165). Transfected cells, including control cells transfected with a random-sequence siRNA construct (Sigma Aldrich), were maintained 48 h at 37°C prior to thioflavin-T staining. To assess amyloid-like aggregates, siRNA-treated cells were incubated with 0.1% (w/v) thioflavin-T in phosphate-buffered saline, and imaged in a Keyence automated-stage fluorescence microscope. Total aggregate fluorescence per cell was calculated using the Fiji plug-in to ImageJ, as previously described.[6]

RNAi knockdown and chemotaxis assay in a *C. Elegans* AD model

Chemotaxis Index (CI) was assessed in *C. elegans* strain CL2355, expressing human $A\beta_{1-42}$ in all neurons as previously described.[43,44] Briefly, prior to chemotaxis assay, eggs from age-synchronized cohorts of worms were hatched and fed with *E. coli* bacteria (HT115/DE3) carrying a plasmid that harbors either empty feeding vector (FV) or a construct yielding RNAi targeting the gene of interest.[2,45] Worms were maintained

at 20°C to assess progressive Aβ aggregation and loss of chemotaxis.[2,7] The Day 1 adults were transferred onto plates containing 2-μM FuDR to prevent progeny production and incubated at 25°C to induce Aβ production. Day 5 (post-hatch) worms were collected after serial washes to remove progeny in larval stage and residual bacteria, and were assayed as previously described[11] in 100-mm culture dishes. Briefly, worm motility toward 1-butanol (chemotaxis) was scored after 2 h and the 'Chemotaxis Index' (CI) was calculated as a normalized response.

Thioflavin-T staining of amyloid-like aggregates in SY5Y-APP$_{Sw}$ cells

To quantify amyloid-like aggregates in SY5Y-APP$_{Sw}$ cells (expressing the "Swedish" double mutant of APP, a model of heritable AD), cells were fixed in formaldehyde and stained with thioflavin-T as described previously.[6] Briefly, before RNAi KD, cells at 70–80% confluence were detached in trypsin/EDTA and sub-cultured in triplicate wells of 96-well plates (at 5,000–8,000 cells/well) containing antibiotic-free DMEM medium with 10% v/v FBS (Invitrogen). At 6-h post-plating, the gene of interest (or vehicle alone) was transfected into SY5Y-APP$_{Sw}$ cells with Lipofectamine 3000 (ThermoFisher) and maintained at 37°C for 48 h. Cells were then fixed in 4% v/v formaldehyde and incubated with 0.1% (w/v) Thioflavin T in phosphate-buffered saline (PBS) along with DAPI. Fluorescence intensities of images captured on a Keyence (BZ-x810) microscope were quantified using FIJI (ImageJ) software.[46]

QUANTIFICATION AND STATISTICAL ANALYSIS

Significance of differences between groups was assessed by homoscedastic "Student's" *t* tests for groups of N > 8 with like variance; for smaller groups or groups of unequal variance, the heteroscedastic *t* test (Excel option 3) was employed. Differences in proportions were assessed for significance by chi-squared tests or Fisher's exact tests, as appropriate to group sizes. In some analyses, multiple repeat assays were treated as individual points and significance ascertained by heteroscedastic *t* tests. Benjamini-adjusted significances of annotation-term enrichment were calculated by DAVID (https://david.ncifcrf.gov/home.jsp, Dec. 2022) as *p* values corrected for multiple endpoints. All tests were 2-tailed except (as noted) if the direction of a significant shift had been previously determined.